Distribution and availability of rare earth elements and trace elements in the estuarine waters of the Ría of Huelva (SW Spain)

Carlos Ruiz Cánovas[1]*, Maria Dolores Basallote[1], Francisco Macías[1]

* Corresponding autor: carlos.ruiz@dgeo.uhu.es

1. Department of Earth Sciences and Research Center on Natural Resources, Health and the Environment, University of Huelva, Campus 'El Carmen', Fuerzas Armadas s/n, 21071 Huelva, Spain.

Abstract

Metal pollution in estuaries represents a serious environmental challenge, especially in areas affected by industrial and mining activities. This study investigates the metal partitioning and availability of rare earth elements (REE), Y and other trace metals (Ag, Tl, U and Cs) in the Ria of Huelva estuary (SW Spain), strongly affected by mining and industrial activities. A 30h monitoring campaign was performed collecting periodic water samples and deploying diffusive gradient in thin films (DGTs) devices to determine the main factors controlling metal availability. The dissolved concentrations of U (3118-3952 ng/L) and Cs (284-392 ng/L) were in the same order of magnitude than those reported in other estuaries and coastal waters worldwide, however, REE (26 -380 ng/L), Y (15-109 ng/L), Ag (14-307 ng/L) and Tl (29-631 ng/L) concentrations exceeded these values for the same salinities. Unlike most metals (i.e. Ag, Tl, U, Cs), which were mainly found in the dissolved form (87-100% of total), REE and Y were found in the particulate phase (22-36% of total). Metal lability was mainly related to the concentration in the water column following this order: U>REE>Y>Ag>Tl. A similar binding mechanism was observed for Tl and Cd, due to its chemical affinity. This relationship between chemical properties and absorption by DGT-resin was also observed for REE (and Y), Rb and Sr, which may cause bioaccumulation upon persistent exposure, considering the ability of these metals to cross the biological membranes. The lability of metals predicted by geochemical codes did not coincide with absorption of labile metals by DGTs due probably to the instability of complexes in contact with the DGT membranes, the inability of metals to form thermodynamically stable complexes or the absorption of

colloids. From this work it can be concluded that DGT passive sampling should complement traditional sampling to monitor metal availability in aquatic environments.

Capsule:

Metal retention (i.e. REE, Y, Ag, Tl, U, Cs) in a strongly polluted estuary by Diffusive Gradient in Thin Films (DGT) was related to water concentration rather than lability

Keywords; diffusive gradients in thin films (DGT); metal pollution; availability; metal partitioning; sulfide oxidation; labile metals

1. Introduction

Estuaries are endangered coastal bodies due mainly to anthropogenic inputs from river catchments. Metal/loid pollution in estuaries represents a serious environmental challenge, especially in areas affected by industrial and mining activities (Machado et al., 2016). In this context, the pattern of anthropogenic metal emissions has changed in the last years due to the rising production and emissions of technology metals, those in demand, available, and used for the purposes of furthering technology and engineered systems (Eggert 2011). A remarkable example of technology metals is the rare earth elements (REE) and Y, a group of chemically similar metallic elements (i.e. lanthanide series), which are of great importance in the development of emerging key technologies, electronics or the aerospace industry (Chakhmouradian and Wall, 2012). The REE and Y distribution and fractionation processes have been widely studied in estuarine systems (e.g. Lawrence and Kamber, 2000; Nozaki and Alibo, 2003), however, little is known about the bioavailability of REE and Y in estuarine waters. Although some studies report potential toxic effects of REE and Y on aquatic living organisms (e.g. Oral et al., 2010; Romero-Freire et al., 2019), there are some discrepancies in the ecological risk assessment of these metals (González et al. 2014). In addition, some ecotoxicological studies fail to reproduce in the laboratory the real conditions found in the field (e.g. matrices and concentrations). An alternative technique to study REE and Y exposure in aquatic organisms is the diffusive gradient in thin-films (DGT), which provides reliable and sensitive in-situ measurements of DGT-labile metal species (Menegário et al., 2017).

Thus, the use of DGTs allows to better understand the processes that govern interaction of living organisms-biological membranes with labile metal(loid)s, by performing in-situ measurements during a determinate period. Considering that the labile metal fraction retained in the DGT devices may mimic the metal absorption by biological membranes, the use of DGT technique could provide a reliable insight into the bioavailability of REE and Y in aquatic environments. Although previous works have focused on the use of passive samplers like DGT for base metal(loid)s monitoring in estuaries (e.g. Montero et al., 2012; Mangal et al., 2016), to our knowledge, data of REE and Y retention by DGTs in estuaries have not previously reported in literature. In the same way than for REE and Y, the distribution in estuarine waters of other elements such as Ag, Tl, U and Cs have also been, to a greater or lesser extent, focus of research (e.g. Luoma et al., 1995; Windom et al., 2000; Anagboso et al., 2013; Bera et al., 2015). However, the knowledge about the bioavailability of these metals is, like in the case of REE and Y, still limited, especially regarding the use of DGT for measuring these metals in estuarine waters.

In this sense, because the high biological productivity of estuaries, the bioavailability of these metals and their speciation should be assessed, especially in those estuaries strongly impacted by mining and industrial effluents. An outstanding example of such polluted environment is the Ria of Huelva estuary (SW Spain), historically affected by sulfide mining activities. The dissolution of host rocks during sulfide oxidation processes may also release elements such as REY, U, Cs and Tl (e.g. Law and Turner, 2011; Barbero et al., 2014) into the hydrosphere, although this latter metal is moreover associated to sulfides (Lis et al., 2003). Nevertheless, these elements are not only delivered by riverine inputs but also by industrial activities; for instance, around 4.2 ton/yr of U and 144 kg/yr of REE and Y are released from a nearby phosphogypsum stack (Fig. 1) (Pérez-López et al., 2016; Cánovas et al., 2018). For this reason, the Ria of Huelva estuary could be an ideal setting to study the bioavailability of these metals in polluted estuaries worldwide. Therefore, the main aim of this work is to study the metal partitioning and availability of REE and Y and other less studied trace metals (i.e. Ag, Tl, U and Cs) in an estuary strongly affected by mining and industrial activities, as well as unravelling the main factors controlling such bioavailability.

2. Methodology

2.1. Description of the study area

The Huelva estuary, also known as the Ria of Huelva (SW Spain), is formed by the confluence of both the Odiel and Tinto acid rivers (pH average 3.5 and 2.5, respectively) with seawater (Fig. 1). The estuary was cut into unconsolidated Cenozoic sediments during the late Pleistocene and early Holocene. After flooding during the Holocene transgression (around 8700 years BP), the lowest unit of the Holocene estuarine infilling commenced deposition, but the estuary is now entirely infilled with sediment and has started to prograde to form a delta (Carro et al., 2020). Freshwater inflow into the estuary exhibits significant seasonal and annual variations, with average monthly inflows of 49.8 Mm^3 of acidic and metal-rich waters (Carro et al., 2020). The water depth decreases progressively from the upper to the lower part of the estuary, with maximum depths of 13 m. The estuary is characterized by a semidiurnal mesotidal regime with a mean tidal range of 2.69 m (Borrego et al., 2004) and two different mixing processes: (i) a pH-induced mixing process in the upper part, and (ii) a salt-induced mixing in the lower part of the estuary. Thus, the hydrochemical properties of the Ria of Huelva estuary are strongly controlled by mixing processes between the volume of acidic river waters and seawater.

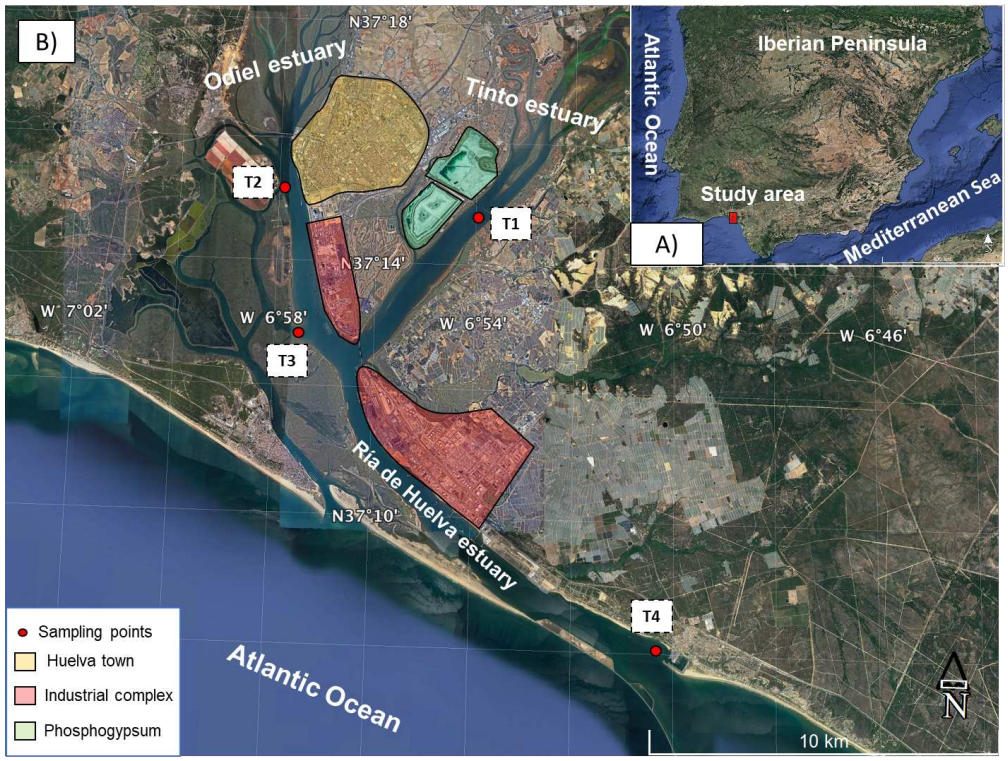

Figure 1. Location map of the study area (A), showing the sampling stations (T1-T4) and main anthropogenic activities (B).

In addition to chronic mining contamination, especially during the last 200 years, the estuary has also suffered from industrial pollution after the settlement of a huge industrial complex in the 60's of the last century, composed mainly of a phosphate fertilizer plant, a pyrite roasting and copper smelting plant, a paper mill and a petrochemical complex (Sainz et al., 2004). In addition, the dumping of around 100 Mt of phosphogypsum (Fig. 1) constitutes an important source not only of base metal/loids into the estuary (Pérez-López et al., 2016) but also of REE and Y (Cánovas et al., 2018).

2.2. Sampling

A synoptic water sampling (n= 16) was performed during a 30h-time span (0, 6, 24, and 30h on July 25-26th 2018) along the outer zone of the Ria of Huelva estuary, where a greater biological diversity is found. The time span was selected in order to include several tidal cycles (low and high tides) to study the metal distribution and exposure associated with these tidal changes. The tidal range during the study period was 1 m, reflecting micro-tidal conditions in the estuary. Four different sampling stations were selected according to their proximity to mine water influence and/or industrial and harbor activities (Fig. 1) in order to evaluate their contribution. Sampling points were selected within the outer zone of the estuary, dominated by salt-induced mixing processes and near-neutral pH values, and characterized by abundance of living organisms and by being affected by anthropogenic activities. T1 is located in the Tinto estuary and suffers from both mining (Tinto river) and industrial effluents (acidic and metal-rich leachates from the phosphogypsum stack; Fig. 1). Located in the outer part of the Odiel estuary, T2 and T3 suffer from mining influence by the Odiel river, although T3 may be also impacted by the Tinto river during high tides (Fig. 1) and by recreational boat activities. Lastly, T4 is the outermost sampling point within the Ria of Huelva estuary, where seawater influence is greater, being also affected by a harbor for recreational ships (Fig. 1). The toxicity of the sediments around this area by Cu, As, Pb, and Zn has been previously reported (Basallote et al., 2018).

146 Water samples (n=16) for trace elements determination were collected in high-density
147 polyethylene (HDPE) bottles, filtered through cellulose nitrate 0.45 µm pore size
148 Millipore filters, acidified to pH < 2 with Merck Suprapur® nitric acid 65% and kept stored
149 at 4 ºC until analysis. Raw samples (not filtered but acidified) (n=16) were also collected
150 to determine the metal particulate content, being the difference between the filtered
151 and unfiltered samples assumed to be associated with particulate matter. A third aliquot
152 was collected and filtered but non-acidified for anion determination. All HDPE bottles
153 used during the sampling were acid-washed (10% HCl) for 24 h, rinsed in milli-Q water
154 and stored in sterile bags prior to use.
155
156 Potential metal toxicity and bioavailability was studied by passive samplers. Thus,
157 diffusive gradient in thin-films (DGT) devices (LSNX-NP loaded DGT device; DGT®
158 Research) were deployed in sampling points by duplicates. DGT units were deployed
159 hanging at 1 m depth bellow water surface using nylon cords to support them. The used
160 Chelex binding gel DGTs have been widely used for the determination of up to 40 metals
161 (Panther et al. 2014). In these devices, free cations and metal complexes are diffused
162 through a cellulose nitrate filter (0.45 µm porosity) and a diffusive gel due to a
163 concentration gradient, and then accumulated in a chelating resin gel Chelex-100. After
164 12 and 24h of exposure, DGT devices were removed and carried to the laboratory in
165 sterile bags. Then, the DGTs were disassembled and each resin gel (Chelex 100-gel) was
166 immersed separately in 1 mL ultrapure HNO_3 (3M) contained in acid washed
167 polyethylene vials and agitated at 60 rpm for 24 h, according to a specific determination
168 protocol (Ardelan et al., 2009; Basallote et al., 2020). Afterwards, the elution extracts
169 were diluted with Milli-Q water (18.2 MΩ, Millipore) to 10 mL, before metal
170 determination. Laboratory DGT blanks were used for results comparison purpose. DGT
171 concentrations were determined according to Davison and Zhang (1994) using Eq. (1):

172 $$C_{DGT} = \frac{MDGT\Delta g}{DtA}, \qquad \text{Eq. (1)}$$

173 where C_{DGT} is the concentration of metal in the DGT extract, M_{DGT} is the mass of the
174 metal accumulated on the binding layer, Δg is the thickness of the diffusive gel (0.078
175 cm) plus the thickness of the filter membrane used (0.014 cm), D is the diffusion
176 coefficient of each metal ($cm^2\ s^{-1}$), t is deployment time (s, exact time for each exposure

period), and A is the DGT cross-sectional exposure area (3.14 cm^2). The REE, Y and Tl diffusion coefficients (D) reported by Yuan et al. (2018) and Deng et al. (2019) respectively, were used in this study, taking into account the average temperature.

2.3. Analytical determinations

Physico-chemical parameters (i.e. temperature, pH, electrical conductivity (EC), and oxidation-reduction potential (ORP)) were measured in situ using a HANNA HI 98190 and 98192 portable meters. A three-point calibration was done for both EC (1.413, 12.88, and 80 mS/cm) and pH (4.01, 7.00, and 9.21), while ORP was controlled using two points (240 and 469 mV). The salinity (S) of samples was calculated from the Cl^- content (following the equation $S = 1.805\ Cl^-\ (g/L) + 0.03$; from Chester, 1990). The concentration of major elements (i.e. Na, Ca, Mg, and K) was determined by ICP-OES (Jobin Yvon Ultima 2). Trace metal/loid determination in water samples and DGT elution extracts was performed in triplicate by iCAP TQ ICP-MS at the HydroSciences laboratory of the University of Montpellier (Tables SM1 and SM2). Raw samples were 0.45 µm pore size filtered prior to analyze them to avoid any particle interference. Detection limits ranged from 0.1 to 2.0 ng/L for REE and Y, 2 ng/L for Ag, 1 ng/L for Cs, 0.4 ng/L for Tl and 0.3 ng/L for U (Table SM2). Blanks were analyzed for both water and DGT extract samples. Estuarine water reference material for trace metals (SLEW-3) was also analyzed to verify the analytical accuracy. In addition, anions (i.e. PO_4^{3-}, Br^-, Cl-, NO_3^-, NO_2^-, and F) determination was performed by ion chromatography (Dionex DX-120) at the R+D laboratories of the University of Huelva while total alkalinity was determined by CHEMetrics® Total Titrets®, with a range of 10–100 or 100–1000 mg/L as $CaCO_3$ equivalents. The quality of anion determinations was validated by home-made standards.

2.4. Data treatment

REE concentrations were normalized using the North-American Shale Composite (NASC) values (Gromet et al., 1984) to study fractionation processes during metal partitioning along the estuary and uptake by living organisms. Cerium $(Ce/Ce^*)_{NASC}$ and Europium $(Eu/Eu^*)_{NASC}$ anomalies were also determined from the expression $Ce_{NASC} / \sqrt{[La_{NASC} \cdot Pr_{NASC}]}$ and $Eu_{NASC} / \sqrt{[Sm_{NASC} \cdot Gd_{NASC}]}$ from Worrall and Pearson (2001) and Taylor and

McLennan (1985), respectively. DGT results were compared with speciation modelling to interpret and validate these measurements. Thus, chemical speciation and saturation indices of solutions were calculated by PHREEQC code v3.4 (Parkhurst and Appelo, 2013) using the database provided by Lawrence Livermore National Laboratory (llnl.dat), based on Truesdell-Jones equations. Collected samples exhibited values of ionic strength below 0.7. Information provided by PHREEQC was compared with chemical speciation obtained using the CHEAQS program version 2017.3 (Verweij, 2017) for the sake of consistency. The CHEAQS model includes inorganic speciation and mineral equilibrium based on the National Institute of Standards and Technology database version 8.0 (NIST, 2004).

3. Results

3.1. Dissolved REE, Y and trace metal concentration in water samples

Estuarine waters studied shown mean pH values of 8.2, salinity of 34 g/L and concentrations of 23 g/L of Cl^-, 9.0 g/L of Na, 3.5 g/L of sulfate, 1.0 g/L of Mg, 469 mg/L of K, 327 mg/L of Ca and 100 mg/L of Br (Table SM1). In addition, mean dissolved concentrations of 65 µg/L of Mn, 50 µg/L of Zn, 21 µg/L of Cu, 14 µg/L of Fe and lesser values of other metal/loids were observed in the estuarine waters (Table SM1).

Concerning REE and Y, dissolved concentrations in the estuarine waters ranged from 26 to 380 ng/L and from 15 to 109 ng/L, respectively (n=16; Table SM2) with the maximum values observed in T2 (Fig. 2). There is no a clear tendency of decreasing or increasing concentrations along the estuary, although generally higher concentrations were observed at low tides (Fig. 2), probably due to the higher influence of AMD. The dissolved concentrations of other trace metals such as Ag and Tl were found in the same order of magnitude than REE and Y; Ag concentrations ranged from 14 to 307 ng/L (mean value of 135 ng/L; Table SM2) while Tl concentrations varied from 29 to 631 ng/L (mean value of 225 ng/L; Table SM2). However, a different evolution is observed for these elements; while Tl concentration decreased progressively concomitantly to the seawater influence and oscillations associated with tides, Ag concentration followed an

239 uneven evolution and tide-associated variations were only observed in T1 (Fig. 2). In
240 addition, higher values for Tl were observed at low tides, especially in T1 and T2.

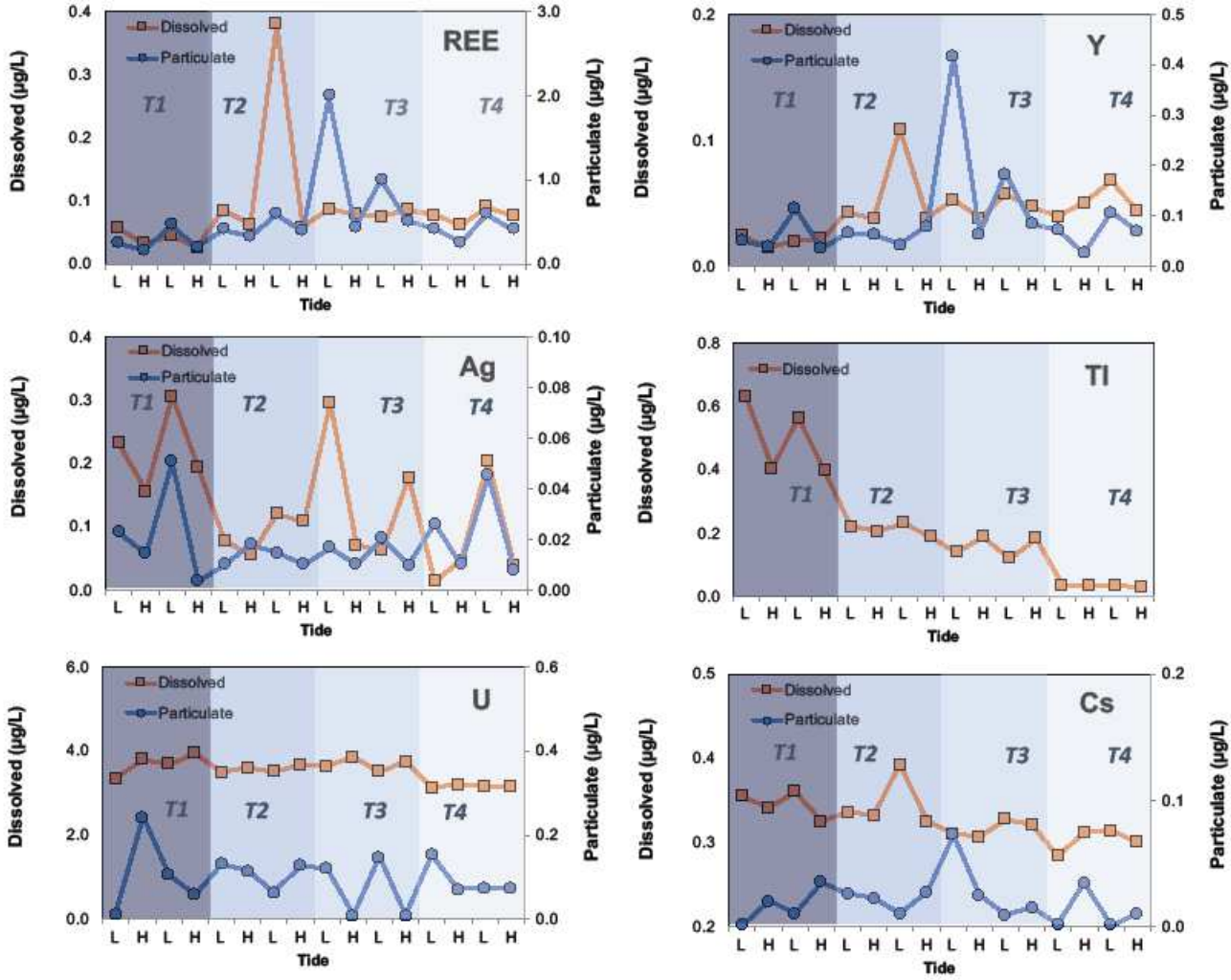

241

242 **Figure 2.** Evolution of dissolved (orange square) line) and particulate (blue circle)
243 concentrations of metals in the estuary for the 4 sampling sites (T1, T2, T3 and T4) and
244 for the 4 sampling times (L: low tide; H: high tide). Particulate Tl concentrations were
245 below detection limit of the equipment.

246

247 Dissolved Cs and U concentrations showed a lower variability than the rest of trace
248 elements (i.e. REE, Y, Ag and Tl), although values for U were an order of magnitude
249 higher than for Cs; U concentration varied from 3118 to 3952 ng/L (mean value of 3525
250 ng/L), whereas the Cs concentration ranged from 284 to 392 ng/L (mean value of 327
251 ng/L; Table SM2). Both metal concentrations followed a slightly progressive decrease in
252 the estuary associated with seawater influence, although in the case of Cs the maximum

concentration among sites was observed in T2, at low tide conditions, similarly to REE and Y (Fig. 2).

3.2. Particulate REE, Y and trace metal concentration in water samples

The particulate concentration of REE and Y is noticeably higher than dissolved (Table SM2 and Fig. 2); particulate REE and Y ranged from 129 to 591 ng/L, and from 27 to 175 ng/L, respectively (mean values of 437 and 95 ng/L), with maximum values observed in T3 at high tides (Fig. 2). The average particulate concentration of U was 95 ng/L, with maximum values of 244 ng/L (Table SM2). Lower values were observed for Cs and Ag (mean concentration of 20 and 18 ng/L, respectively), while no particulate Tl was found in collected samples. No clear trends in particulate concentration of metals were observed neither associated to seawater influence nor tides, except in the case of REE and Y with higher values at low tides, especially in T1 and T2 (Fig. 2). The distribution pattern of metals studied is clearly defined in Figure 3; REE and Y are mainly found in the particulate phase, travelling in this form outside the estuary, with an average of 78% and 64% of total REE and Y, respectively (Fig. 3).

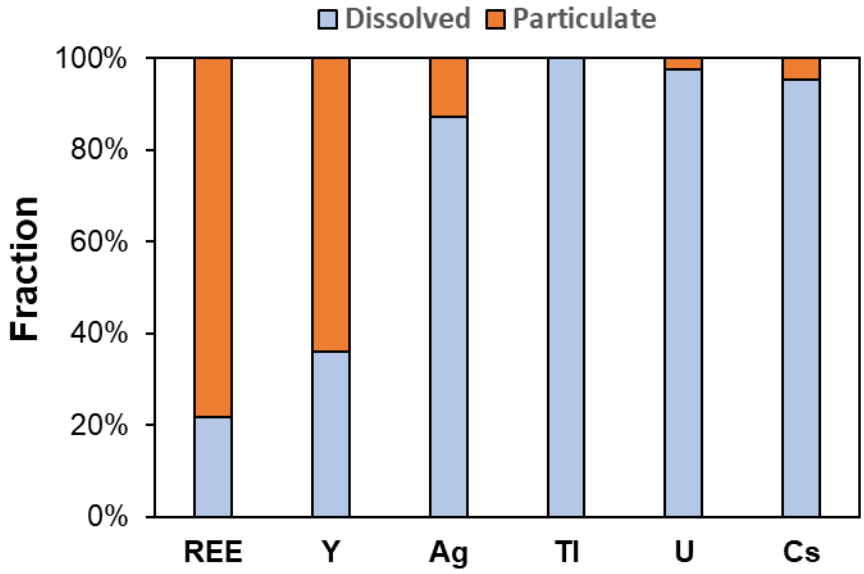

Figure 3. Percentage of the dissolved and particulate fraction for each metal studied.

Unlike REE and Y, the rest of metals studied was preferentially present in the dissolved phase (Fig. 3), with values of dissolved fraction ranging from 100% for Tl to 87% for Ag.

3.3. Metal concentration in the DGT devices

The metal concentrations in DGT (C_{DGT}) deployed in the sampling stations is shown in Table SM2. As can be seen, the element displaying higher concentrations in the DGTs was U, with values ranging from 1053 to 1771 ng/L (Table SM2). Lower C_{DGT} values were observed for REE and Y, ranging from 62 to 208 ng/L, and 18 and 74 ng/L, respectively (mean values of 114 and 41 ng/L, respectively). The average concentration of Tl and Ag in DGTs was 11 and 21 ng/L, respectively with maximum values for Ag of up to 127 ng/L (Table SM2). On the other hand, Cs concentrations in the DGTs were below the detection limit.

4. Discussion

4.1. Comparison with other estuarine systems worldwide

The estuarine waters studied reflect the area where almost complete mixing of alkaline seawater with acidic river waters of the Tinto and Odiel rivers takes place. As a consequence of the progressive increment of pH and salinity values in the mixing zone, a net transference of most metals from the water column to the particulate matter and subsequently their settlement into the estuarine sediments occur (Elbaz-Poulichet et al., 2001). Only the most mobile metals (e.g. Zn, Cu and Cd) pass through the estuary giving rise to a metal-rich plume in the coastal waters of the Gulf of Cádiz (e.g. Van Geen et al, 1991; Elbaz-Poulichet et al., 2001). Thus, dissolved metal/loid concentrations in sampling points were low if compared to upper sections of the estuary, where low pH values (even below 3) and element concentrations exceeding mg/L are commonly found (Elbaz-Poulichet et al., 2001; Olías et al., 2019). Nevertheless, these values are in some cases several orders of magnitude higher than values reported in other estuaries worldwide (Cánovas et al., 2020). This transference between the aqueous and particulate phases can be evidenced by the high concentration of particulate Fe, with mean values of 178 µg/L, 12 times higher than that of dissolved Fe. The presence of other metals in the particulate matter is also observed, with mean values of 5 µg/L of Mn, 4.9 µg/L of Cu and 2.7 µg/L of Pb (Table SM1).

A comparison with other estuarine systems can be done. For example, REE values are slightly higher than those reported for similar salinities (> 30 g/L) in other polluted estuaries worldwide such as the Amazon (18-26 ng/L of REE; Rousseau et al., 2015) and

Paraguaçu estuaries in Brazil (around 15 ng/L; Andrade et al., 2020) or the Pearl River estuary in China (around 60 ng/L; Ma et al., 2019). In the case of Ag, these values are higher than those previously reported in most European estuaries (Tappin et al., 2010), some of them affected by mining and agriculture activities such as the Fal and Tamar estuaries in UK (2.0 and 3.7 ng/L; Tappin et al., 2010) and the Restronguet Creek (19 ng/L; Tappin et al., 2010) and Gironde estuaries (6-8 ng/L, Lanceleur et al., 2012) in France. On the contrary, values recently reported by Ribeiro et al. (2018) in the Portuguese Douro estuary (i.e. 288-970 ng/L), heavily populated and strongly influenced by anthropogenic activities, exceeded those reported in this study. Regarding Tl, concentrations found in this study (29-631 ng/L) exceeded those reported in other European estuaries such as the Tamar (2-9 ng/L; Anagboso et al., 2013) and Weser (13-30 ng/L; Böning et al., 2017). These enhanced contents of Ag and Tl in this estuary with respect to other European estuaries may be due to the influence of AMD. On the other hand, no anthropogenic inputs of dissolved U and Cs seem to exist since dissolved concentrations reported in this study are quite similar to average oceanic concentrations of 3300 ng/L (Ku et al., 1977) and 306 ng/L (Bera et al., 2015), respectively.

4.2. Metal partitioning in the estuarine waters

The affinity of REE and Y by the particulate phase in estuarine systems has been widely reported (e.g. Sholkovitz, 1995; Lawrence and Kamber, 2006) and attributed to coagulation of iron oxide-organic colloids with which REE are strongly associated. Comparing the particulate concentrations of REE and Y with those observed for other elements also present in the particulate matter in this study (i.e. Fe, Cu, Mn or Pb), a high positive correlation (r^2= 0.93) is observed between REE and Y and particulate Fe (Fig. 4), which point at Fe mineral phases transported outside the estuary as main REE and Y carrier phases. Other metals such as Cu and Zn (the latter not shown in Fig. 4) also showed a good correlation with particulate REE and Y. On the other hand, poorer correlations were observed for other metals such as Mn, and Pb (Fig. 4). These results partially agree well with those of Mihajlovic et al. (2014), who reported that REE in marsh soil profiles were concentrated in the aqua regia extractable fraction, associated to amorphous iron (and manganese) mineral phases. On the other hand, redox

processes associated to water fluctuations may play an important role on metal mobility in estuaries. In this sense, Mihajlovic et al. (2017) reported increasing REE mobility due to pH changes associated to redox-conditions. However, the relative contribution of AMD with respect to seawater may be the cause of REE fluctuations observed in this study (Fig. 2).

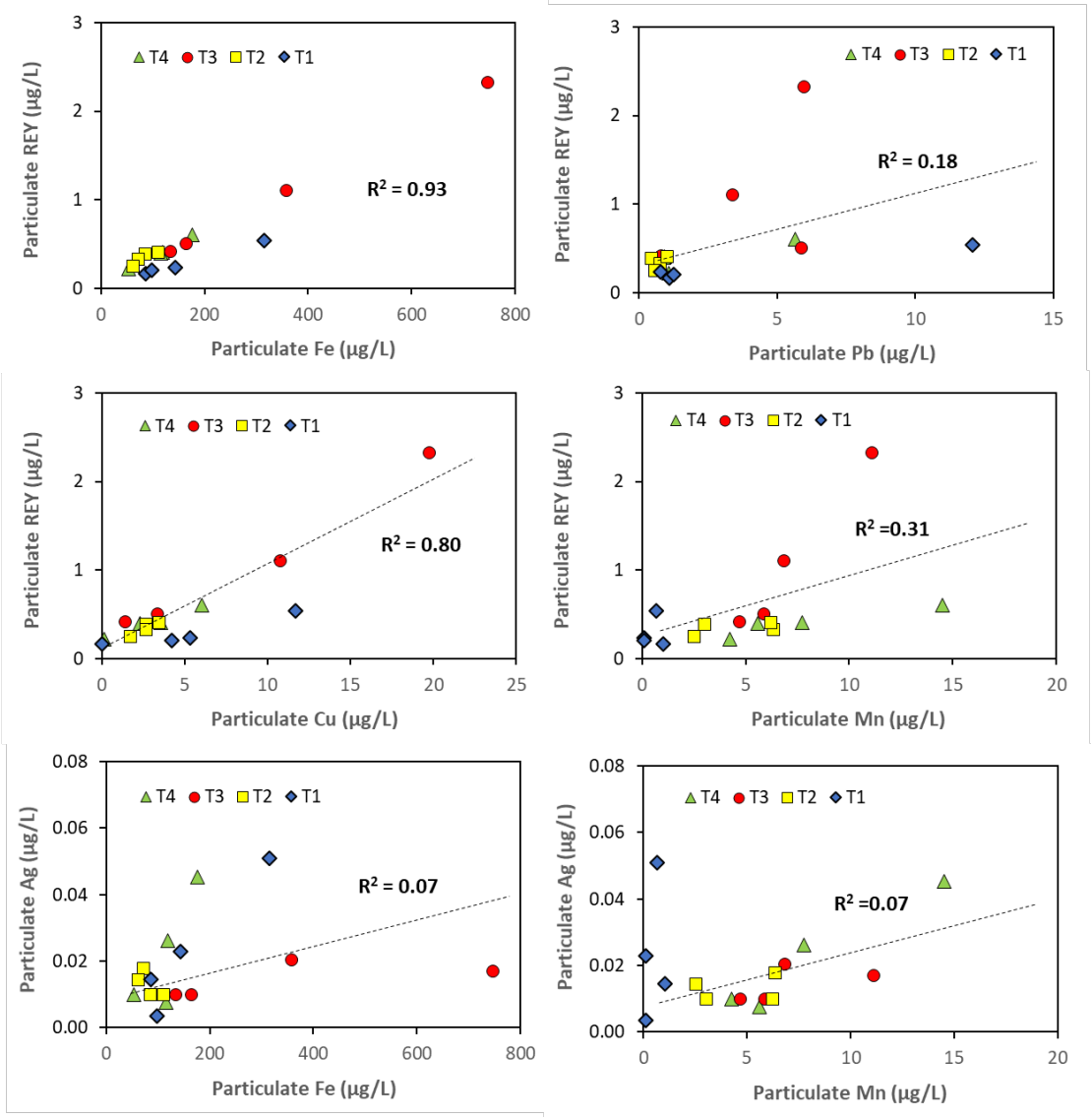

Figure 4. Relationship between the concentration of particulate REE and Y and Ag, and other metals.

Regarding Ag, although it has been reported that around 80% of particulate Ag in the Galveston Bay estuary was associated to Fe/Mn oxyhydroxides (Wen et al., 1997), no correlation between particulate Ag and Fe (neither Mn) was observed in this study (Fig.

4). This absence of correlation may be related to the complexation of Ag in the estuarine waters, dominated by the formation of Cl complexes, which may limit particle-reactivity at salinities above 5 (Luoma et al., 1995). Thus, REE and Y remain associated to Fe-rich colloids along the estuary while Ag may be desorbed from these colloids at increasing Cl concentrations.

4.3. Metal speciation and bioavailability

Although, as previously mentioned, the concentrations of elements such as REE, Y, Ag or Tl observed in this study are noticeably higher than those observed in most European estuaries affected by anthropogenic activities (e.g. Tappin et al., 2010; Anagboso et al., 2013; Böning et al., 2017), their toxicity and mobility depend on both their concentration and speciation (Allen, 1993). Thereby, only the labile fraction of metals is expected to be available for the living organisms (Amato et al., 2014). The retention in the DGT for each element was mainly related to the concentration in the water column. Hence, higher C_{DGT} was observed for those elements showing higher concentration in the dissolved and particulate phases. Since Tl exhibits similar aquatic toxicity and chemical similarities with Cd, Ag and Pb (Turner et al., 2013), an analogous trend in DGT concentrations would be expected for these elements. However, Tl C_{DGT} only exhibits a similar trend to Cd, although the C_{DGT} of this latter metal is higher than that observed for Tl.

This relationship between chemical properties and absorption by the DGT-chelating resin is also observed for REE and Y (Fig. SM1), which exhibited a high correlation (R^2= 0.89). This chemical similarity between each other has been widely reported, in such a way that Y is considered as part of the REE (Chakhmouradian and Wall, 2012). In addition, the C_{DGT} of these elements (i.e. REE and Y) showed a high correlation with the C_{DGT} of other elements (Fig. SM1) such as Rb (R^2= 0.85) and Sr (R^2= 0.92), which commonly cross the biological membranes (Nielsen, 2004; Chowdhury and Blust, 2011). On the other hand, despite having a different chemical behavior, U seems to follow a similar trend of absorption than Tl (and Cd) as evidenced by the correlation between both C_{DGT} (R^2= 0.67).

A comparison of DGT results with speciation modelling by geochemical codes can be a very insightful way to interpret the measurements, in addition to acting as a complementary technique for purposes of data validation (Menegario et al., 2017). The labile fraction is considered as the labile forms of metals including free metal species and weak metal–ligand complexes (Menegario et al., 2017). Generally, those metals that are mostly found as free or weak metal complexes (e.g., Free-Metal, Cl-Metal species) are expected to be more labile than those mainly found as carbonate or hydroxyl complexes (strong ligands). Table SM3 and Figure 5 show the speciation of the metals studied. It is clearly observed that REE (and Y) CO_3-complexes prevail over other species (i.e. free form, Cl-complexes, F-complexes, SO_4-complexes, and O/OH complexes), with values ranging from 60 to 96% of total species. Sulfate (0.01 to 22%), fluoride (0.06% to 8%), free (0.22 to 7%), chloride (0.10 to 2.1%), and O/OH complexes (less than 1%) were of minor importance in REE and Y speciation (Table SM3). A general increase in carbonate complexes is observed across the lanthanide series, with a lower contribution for La (average value of 60%), while the opposite tendency (decreasing across the lanthanide series) is observed for the rest of species (i.e. free, sulfate, fluoride, and O/OH complexes; Fig. 5). Considering the aforementioned lability of species, REE and Y would have a low lability, since the percentage of labile species is below 10% of total (Table SM3). In this sense, it is noteworthy that the increase in carbonate complexes across the series would imply a decrease in lability (from 10% for La to 1% for Lu). A similar lability would be expected for U due to its capacity to form strong complexes in seawater with carbonates such as $UO_2(CO_3)_3^{4-}$and $UO_2(CO_3)_2^{2-}$ (Langmuir, 1978), being the former, the most predominant U species in waters (around 99% of total; Table SM3).

In contrast to REE, Y and U, which were mainly found forming strong complexes (mainly carbonate complexes) and therefore showed a low percentage of labile species (below 10%), Ag, Tl and Cs displayed contents of labile species above 93% of total (Table SM3). These metals would thus exhibit a higher lability according to the determined species (mostly free form and Cl-complexes). For instance, Cs was mainly found as free species (84% of Cs^+) and Cl complexes (16% of CsCl). Lower values of free species were obtained for Tl (average of 43% for Tl^+), in favor of Cl (TlCl and $TlCl_2^-$; 50%, Table SM3) and sulfate complexes (7% of $TlSO_4^+$).

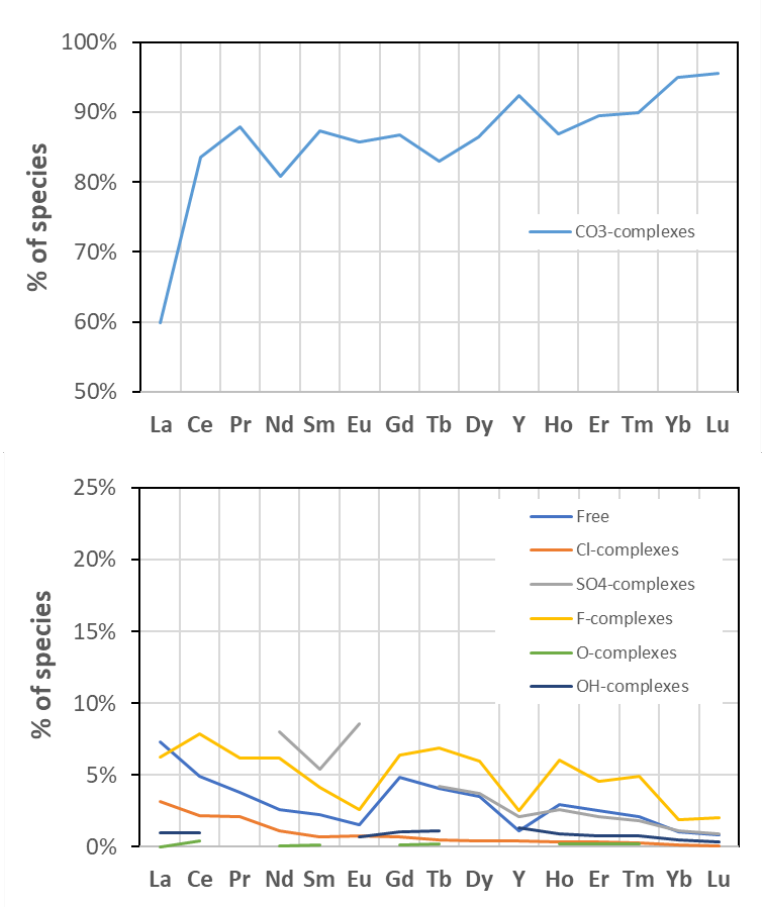

Figure 5. Average speciation values for REE and Y in collected samples.

On the other hand, Ag was chiefly found forming Cl complexes, being $AgCl_4^{3-}$ (around 99% of total; Table SM3) the predominant species. Comparing the percentage of C_{DGT} with respect to the dissolved concentration in the water column (i.e. dissolved+particulate; Table SM2) with their lability (according to speciation modelling; Table SM3), some noteworthy information may be obtained. In this sense, the total concentration was used (instead of dissolved) to represent metal exposure for living organisms since colloidal phase could play a major role in bioavailability, as recently reported by Cánovas et al. (2020), although only REE and Y were mostly found in the particulate matter (Fig. 3). As can be seen in Table SM2, C_{DGT} for REE ranged from 15% to 35% of total concentrations in the water column (average value of 24%), being these values higher for LREE and HREE than for MREE (Table SM2). These values exceed those of labile species (below 10% of total concentrations; Table SM3), although in this case the contribution of particulate REE may increase the REE absorption by DGT, mainly linked to the absorption of Fe colloids (Cánovas et al. 2020). On the other hand, labile

metals such as Ag, Cs and Tl (lability between 93 and 100%) were scarcely retained in the DGTs considering their total concentration in the water column; 15% of Ag and 5% of Tl in water was only retained in the DGTs (Table SM2), while Cs values were below the detection limit in DGT solutions. Such discrepancies have been previously reported by Liu et al. (2013) and attributed to the inability of metals to form thermodynamically stable complexes, leading to a lower binding by the DGT resin layer. An unexpected metal absorption in the DGT devices was also observed for U (40% of U concentration in waters was retained in the DGTs), which should be scarcely labile due to carbonate complexation. Therefore, remarkable discrepancies were observed in this study between the lability of metals and retention by DGTs. Regarding REE and Y, this discrepancy may be related to its presence in the Fe-rich particulate matter and subsequent absorption in the DGTs, as previously commented. However, there is no clear explanation for such high U absorption in DGT. Since U is strongly complexed by carbonates, which may preclude its passing through the filter membrane, it is hypothesized that carbonate complex instability in the membrane surface may cause the release of U and its incorporation into the DGTs. However, this hypothesis must be further tested.

4.4. REE and Y fractionation

Figure SM2 shows the NASC-normalized patterns of dissolved, particulate and DGT concentrations of REE. As can be seen, the NASC-normalized patterns of dissolved REE shows an evident negative Ce anomaly (average value of 0.6, interquartile range of 0.49-0.69). Bau et al. (1999) reported that the development of such anomaly in REE and Y patterns is due to oxidative scavenging, which is especially intense in aqueous systems where fresh Fe oxyhydroxides precipitate. For this reason, the high concentration of these newly-formed minerals in the estuarine waters due to mixing of AMD with seawater (average Fe particulate concentration of 178 µg/L; Table SM1) may favor the formation of this negative Ce anomaly in waters. It is also noteworthy the occurrence of a positive Gd anomaly. This positive Gd anomaly, which has also been previously reported in estuaries affected by anthropogenic inputs (e.g. Nozaki et al. 2000), is attributed to the medical application of Gd for magnetic resonance imaging (Bau and Dulski, 1996).

Previous studies have reported the existence of fractionation processes in estuarine systems (e.g. Lawrence and Kamber, 2000; Nozaki and Alibo, 2003; Andrade et al., 2020). Thus, during estuarine mixing of river waters rich in inorganic nanoparticles and colloids with seawater, LREE may be preferentially partitioned onto suspended particles and colloids while HREE tend to remain in solution due to stronger complexation to dissolved ligands. According to this, an enrichment in HREE in waters should be expected, while particulate matter may be enriched in LREE. However, this fractionation is not so evident in this study. As can be seen, a flatter pattern is observed in the dissolved phase instead (Fig. SM2), with almost neither enrichment in HREE nor depletion in LREE, while an enrichment in MREE is observed in the particulate matter. This absence of the common fractionation pattern could be related to the higher reactivity of Fe mineral phases in this estuary compared to other estuaries worldwide, thus, the precipitation of highly amorphous Fe minerals as a consequence of AMD mixing with seawater may inhibit this preferential incorporation of LREE onto suspended particles and colloids.

Fractionation processes have been also reported in living organisms. In this sense, Akagi and Edamani (2017) studied the REE distribution and fractionation in shells and soft tissues of bivalves from Tokyo Bay. These authors reported that REE patterns in bivalves exhibited a MREE enrichment, resembling that found in particulate matter rather than in the dissolved phase. Other studies reported that REE patterns in oysters coincided with those observed in the suspended particles at the Pearl River estuary (China) (Ma et al., 2019). On the other hand, Wang et al. (2019) reported an enrichment in LREE in different living organism (i.e. fishes, mollusks and crustaceans) in the Maluan Bay (China). Considering that DGT devices may mimic the metal absorption by living organisms, the opposite finding was reported in the Ria de Huelva estuary; an enrichment in HREE was observed in the DGT devices, which does not fit neither the REE patterns of dissolved nor particulate fraction.

4.5. Technical and environmental implications and health risk assessment

Although there are no studies on bioaccumulation of studied metals (i.e. REE, Y, Ag, Tl, Y and Cs) of aquatic organisms in this estuary, some cases are reported in other estuaries

worldwide. In this sense, Wang et al. (2019) studied the bioaccumulation of REE in several species of aquatic organisms in the Maluan Bay (China). These authors reported concentrations in mollusk two orders of magnitude higher than those in fish, exhibiting species-specific accumulation patterns across taxa. However, factors controlling REE and Y absorption by aquatic organisms are not entirely clear. Previous studies indicate that metal absorption by living organisms is directly related to environmental concentrations. For instance, it has been reported that the incorporation of REE in soft tissue of the Asian clam is proportional to the pollution degree in the aquatic environment and preserve the REE geochemical signature found in the environment (Bonnail et al., 2017). In the present study, a direct relationship between metal levels in the water column and absorption was only observed for Tl (R^2= 0.84) and to a lesser extent for U (R^2= 0.75) (Fig. SM3). Although generally higher C_{DGT} are observed at higher concentrations in water, neither REE (and Y) nor Ag showed any relationship between environmental concentrations and metal absorption by DGT (Fig. SM3). In addition, the geochemical signature of REE in DGTs (enrichment of HREE over MREE and LREE) seems not to have been preserved from the environment (enrichment in MREE or flat pattern), except the Ce anomaly inherited from the dissolved fraction (Fig. SM2). This dissimilarity between REE patterns in DGT and the environment could be related to the instability processes of carbonate processes in contact with the DGT membrane, previously commented for U. This would explain the HREE enrichment observed in the NASC normalized pattern, since REE are increasingly complexed by carbonate across the lanthanide series (Fig. SM2). However, this hypothesis must be confirmed in further studies.

Another question to be answered is whether DGT devices are suitable as bioindicators or not. As previously reported by Wang et al. (2019), REE bioaccumulation rates may sharply vary across taxa, depending on the assimilation route of each organism. For instance, Ma et al. (2019) also found high correlations (R^2 = 0.99) between REE concentrations in oysters and in suspended particles, concluding that REE in bivalves may not be a suitable indicator of REE pollution in the dissolved phase but rather in sediments or suspended particles. In the case of Tl, the high correlation observed between the retention by DGTs and the concentration in water (Fig. SM3) support these

528 devices as a good monitoring tool for Tl pollution in estuaries. Turner et al. (2013)
529 indicate that Tl bioaccumulation may be related to its similar geochemical affinity to K,
530 thus, Tl^+ is able to cross cell membranes through K^+ channels. Other metals such as REE
531 and Y may also cross biological membranes, according to their similar incorporation in
532 DGTs as Rb and Sr in this study (Fig. SM1). In the case of Ag, Luoma et al. (1995) reported
533 that the toxicity of Ag is of primary concern in marine environments because
534 bioaccumulation increases so steeply with contamination. This strong bioaccumulation
535 of Ag in estuarine and marine environments may be partially due to the formation of
536 neutral Cl-complexes (AgCl), which are highly bioavailable by its low polarity, facilitating
537 its diffusion across biological membranes (Luoma et al., 1995; Wood et al., 2004).
538 Although Ag C_{DGT} did not correlate well with environmental concentrations, the use of
539 DGTs could be a complementary technique for Ag pollution monitoring. On the other
540 hand, the results obtained for some radionuclide elements such as Cs and U were
541 certainly contradictory. While the more labile Cs was not determined in DGTs extracts,
542 the less labile U was retained in these devices (average value of 41% of the total
543 concentration in the water column; Table SM3). These results indicate that DGT devices
544 are not good indicators for Cs pollution in estuarine waters. On the other hand, the
545 retention of U by DGTs may pose a serious concern for living organisms because of its
546 potential bioaccumulation, especially if background concentrations are exceeded for
547 long periods. In this sense, Geng et al. (2012) reported that the toxicity of U was
548 positively correlated with exposure time
549
550 Another important component concerning the technical suitability of DGT devices as
551 monitoring tool of metal availability is the temporal factor. Figure SM4 compares REE
552 dissolved concentrations obtained by grab sampling with C_{DGT} obtained at 12 and 24h.
553 As can be seen, a different response of DGT is observed if compared to total
554 concentrations. A similar response of total and C_{DGT} is observed in T2 and T3, which
555 would indicate that DGT devices are suitable monitoring tools for REE in estuarine
556 waters. However, a higher retention seems to exist compared to environmental
557 concentrations at 12h in T1 and T4, which may be related to the aforementioned
558 instability of complexes in the membranes. The decrease in DGT concentrations

559 generally decreased at 24h to represent environmental concentrations, which may
560 indicate that these processes are reversible. However, this must be further studied.
561
562 **5. Conclusions**
563 This study deals with the metal partitioning and bioavailability of REE and Y and other
564 less studied trace metals (i.e. Ag, Tl, U and Cs) in the seawater-dominated part of an
565 estuary strongly affected by mining and industrial activities (Ria of Huelva, SW Spain).
566 The dissolved concentration of REE, Y, Ag and Tl in estuarine waters was strongly
567 associated to tides and exhibited values higher than those reported in other polluted
568 estuaries worldwide for the same salinity. By contrast, Cs and U concentrations showed
569 a low variability with mean concentrations similar to average oceanic concentrations.
570 The distribution pattern of metals studied is clearly defined; while REE and Y are mainly
571 found in the particulate phase (average of 78% and 64% of total), the rest of metals were
572 preferentially present in the dissolved phase (values ranging from 100% of total for Tl to
573 87% for Ag). The retention in the DGT for each metal was mainly related to the
574 concentration in the water column (dissolved+particulate) following this order;
575 U>REE>Y>Ag>Tl. In general, the lability of metals predicted by the geochemical model
576 did not coincide with absorption of labile metals by DGTs; prominent labile species such
577 as Ag, Tl or Cs were not strongly retained in the DGT, while less labile metals such as
578 REE, Y or U exhibited a higher absorption in these devices. The ability of REE and Y to
579 substitute common metals crossing the biological membranes (i.e. Na^+, K^+, Rb^+, Sr^{2+}) may
580 lead to bioaccumulation troubles if persistent exposure to these metals is maintained.
581
582 **Acknowledgements**
583 This work was supported by the Spanish Ministry of Economy and Competitiveness
584 through the research projects SCYRE (CGL2016-78783-C2-1-R), CAPOTE (CGL2017-
585 86050-R) and by the CEIMAR Excellence Research Campus through the project CEIMAR-
586 CEIJ-005. M.D. Basallote thanks the Spanish Ministry of Science and Innovation for the
587 Postdoctoral Fellowship granted under application reference IJC2018-035056-I. F.
588 Macías was funded by the R&D FEDER Andalucía 2014-2020 call through the project
589 RENOVAME (FEDER; UHU-1255729). The authors would also like to thank to the
590 Associate Editor Prof. Joerg Rinklebe, Dr. Armstrong-Altrin and other three anonymous

591 reviewers for the support and comments that notably improved the quality of the
592 original paper.
593
594 **References**
595
596 Akagi, T., Edanami, K., 2017. Sources of rare earth elements in shells and soft-tissues of
597 bivalves from Tokyo Bay. Marine Chem. 194, 57-62.
598 https://doi.org/10.1016/j.marchem.2017.02.009.
599
600 Allen, H.E., 1993. The significance of trace metal speciation for water, sediment and soil
601 quality criteria and standards. Sci. Total Environ., 134, 23-45.
602 https://doi.org/10.1016/S0048-9697(05)80004-X
603
604 Amato, E.D., Simpson, S.L., Jarolimek, C.V., Jolley, D.F., 2014. Diffusive gradients in thin
605 films technique provide robust prediction of metal bioavailability and toxicity in
606 estuarine sediments. Environ. Sci. Technol. 48, 4485–4494.
607 https://doi.org/10.1021/es404850f.
608
609 Anagboso, M.K., Turner, A., Braungardt, C., 2013. Fractionation of thallium in the Tamar
610 estuary, south west England. J. Geochem. Explor. 125, 1-7.
611 https://doi.org/10.1016/j.gexplo.2012.10.018.
612
613 Andrade, R.L.B., Hatje, V., Pedreira, R.M.A., Böning, P., Pahnke, K., 2020. REE
614 fractionation and human Gd footprint along the continuum between Paraguaçu River to
615 coastal South Atlantic waters. Chem. Geol. 532, 119303.
616 https://doi.org/10.1016/j.chemgeo.2019.119303.
617
618 Ardelan, M.V., Steinnes, E., Lierhagen, S., Linde, S.O., 2009. Effects of experimental CO_2
619 leakage on solubility and transport of seven trace metals in seawater and sediment. Sci.
620 Total Environ. 407, 6255-6266. https://doi.org/10.1016/j.scitotenv.2009.09.004.
621

622 Barbero, L., Gásquez, M., Bolívar, J.P., Casas-Ruiz, M., Hierro, A., Baskaran, M., Ketterer,
623 M.E., 2014. Mobility of Po and U-isotopes under acid mine drainage conditions: an
624 experimental approach with samples from Río Tinto area (SW Spain). J. Environ.
625 Radioact. 138, 384–389. https://doi.org/10.1016/j.jenvrad.2013.11.004.
626
627 Basallote, M.D., Rodríguez-Romero, A., De Orte, M.R., DelValls, T.A. and Riba, I., 2018.
628 CO2 leakage simulation: effects of the pH decrease on fertilisation and larval
629 development of Paracentrotus lividus and sediment metals toxicity. Chemistry and
630 Ecology, 1-21. https://doi.org/10.1080/02757540.2017.1396319.
631
632 Basallote, M.D., Borrero-Santiago, A.R., Cánovas, C. R., Hammer, K. M., Olsen, A. J. and
633 Ardelan, M.V., 2020. Trace metal mobility in sub-seabed sediments by CO2 seepage
634 under high-pressure conditions. Sci. Total Environ. 700, 134761.
635 https://doi.org/10.1016/j.scitotenv.2019.134761.
636
637 Bau, M., Dulski, P., 1996. Anthropogenic origin of positive gadolinium anomalies in river
638 waters. Earth Planet. Sci. Lett. 143, 245–255.
639
640 Bau, M., Dulski, P., 1999. Comparing yttrium and rare earths in hydrothermal fluids from
641 the Mid-Atlantic Ridge: Implications for Y and REE behaviour during near-vent mixing
642 and for the Y/Ho ratio of proterozoic seawater. Chem. Geol.,155 (1-2), 77-90.
643 https://doi.org/10.1016/S0009-2541(98)00142-9.
644
645 Bera, G., Yeager, K.M., Shim, M., Shiller, A.M., 2015. Anthropogenic stable cesium in
646 water and sediment of a shallow estuary, St. Louis Bay, Mississippi. Estuar. Coast. Shelf
647 Sci. 157, 32–41. http://dx.doi.org/10.1016/j.ecss.2015.02.004.
648
649 Böning P., Ehlert C., Niggemann J., Schnetger B. and Pahnke K., 2017. Thallium dynamics
650 in the Weser estuary (NW Germany). Estuar. Coast. Shelf Sci. 187, 146–151.
651 http://dx.doi.org/10.1016/j.ecss.2016.12.004.
652

653 Bonnail, E., Pérez-López, R., Sarmiento, A.M., Nieto, J.M., DelValls, T.A., 2017. A novel
654 approach for acid mine drainage pollution biomonitoring using rare earth elements
655 bioaccumulated in the freshwater clam Corbicula fluminea. J. Hazard Mater. 338, 466-
656 471. https://doi.org/10.1016/j.jhazmat.2017.05.052.
657
658 Borrego, J., López-González, N., Carro, B., 2004. Geochemical signature as
659 paleoenvironmental markers in Holocene sediments of the Tinto River estuary
660 (Southwestern Spain). Estuar. Coast. Shelf Sci. 61, 631–641.
661 https://doi.org/10.1016/j.ecss.2004.07.004.
662
663 Braungardt, C.B., Achterberg, E.P., Elbaz-Poulichet, F., Morley, N.H., 2003. Metal
664 geochemistry in a mine-polluted estuarine system in Spain. Appl. Geochem. 18, 1757–
665 1771. https://doi.org/10.1016/S0883-2927(03)00079-9.
666
667 Cánovas, C.R., Olías, M., Nieto, J.M., Sarmiento, A.M., Cerón, J.C., 2007.
668 Hydrogeochemical characteristics of the Tinto and Odiel Rivers (SW Spain). Factors
669 controlling metal contents. Sci. Total Environ., 373, 363–382.
670 https://doi.org/10.1016/j.scitotenv.2006.11.022.
671
672 Cánovas, C.R., Macías, F., Pérez López, R., Nieto, J.M., 2018. Mobility of rare earth
673 elements, yttrium and scandium from a phosphogypsum stack: environmental and
674 economic implications. Sci. Total Environ 618, 847–857.
675 https://doi.org/10.1016/j.scitotenv.2017.08.220.
676
677 Cánovas, C.R., Basallote, M.D., Borrego, P., Millán-Becerro, R., Pérez López, R., 2020.
678 Metal partitioning and speciation in a mining-impacted estuary by traditional and
679 passive sampling methods. Sci Total Environ 722, 137905.
680 https://doi.org/10.1016/j.scitotenv.2020.137905.
681
682 Carro B., Borrego J., Morales J.A., 2018. Estuaries of the Huelva Coast: Odiel and Tinto
683 Estuaries (SW Spain). In: Morales J. (eds) The Spanish Coastal Systems. Springer, Cham.
684 Springer Nature Switzerland. https://doi.org/10.1007/978-3-319-93169-2_23.

685

686 Chakhmouradian, A.R., Wall, F., 2012. Rare Earth Elements: minerals, mines, magnets
687 (and more). Elements 8:333–340. https://doi.org/10.2113/gselements.8.5.333.
688

689 Chester, R., 1990. Marine Geochemistry. The University Press, Cambridge.
690

691 Chowdhury, M. J., & Blust, R. (2011). 7 - Strontium. In C. M. Wood, A. P. Farrell & C. J.
692 Brauner (Eds.), Fish Physiology (Vol. 31, pp. 351-390): Academic Press.
693 https://doi.org/10.1016/S1546-5098(11)31029-1.
694

695 Davison, W., Zhang, H., 1994. In-situ speciation measurements of trace components in
696 natural waters using thin-film gels. Nature 367, 546–548.
697

698 DelValls, T.A., Saenz, V., Arias, A.M., Blasco, J., 1999. Thallium in the marine
699 environment: first ecotoxicological assessments in the Guadalquivir estuary and its
700 potential adverse effect on the Donana European nature reserve after the Aznalcollar
701 mining spill (SW Spain). Cien. Mar. 25, 161–175.
702

703 Deng, H., Luo, M., Shi, X., Williams, P.N., Li, K., Liu, M., Fan, W., Xiao, T., Chen, Y., Ma,
704 L.Q., Luo, J., 2019. Novel in situ measurement of thallium in natural waters based on the
705 diffusive gradients in thin-films technique containing a delta-MnO2 gel layer. Anal.
706 Chem. https://doi.org/10.1021/acs.analchem.8b03352.
707

708 Eggert, R.G, 2011. Minerals go critical. Nature Chemistry 3, 688–691.
709 doi:10.1038/NCHEM.1116.
710

711 Elbaz-Poulichet, F., Dupuy, C., 1999. Behaviour of rare earth elements at the freshwater-
712 seawater interface of two acid mine rivers: the Tinto and Odiel (Andalucia, Spain). Appl.
713 Geochem. 14, 1063–1072. https://doi.org/10.1016/S0883-2927(99)00007-4.
714

715 Elbaz-Poulichet, F., Morley, N.H., Beckers, J.M., Nomerange, P., 2001. Metal fluxes
716 through the Strait of Gibraltar: the influence of the Tinto and Odiel rivers (SW Spain).
717 Mar. Chem. 73, 193-213. https://doi.org/10.1016/S0304-4203(00)00106-7.
718
719 Geng, F., Hu, N., Zheng, J.F., Wang, C.L., Chen, X., Yu, J., Ding, D.X., 2012. Evaluation of
720 the toxic effect on zebrafish (Danio rerio) exposed to uranium mill tailings leaching
721 solution. J. Radioanal. Nucl. Chem. 292, 453-463. https://doi.org/10.1007/s10967-011-
722 1451-x.
723
724 González, V., Vignati, D.A.L., Leyval, C., Giamberini, L., 2014. Environmental fate and
725 ecotoxicity of lanthanides: Are they a uniform group beyond chemistry? Environ. Int.
726 71, 148–157. http://dx.doi.org/10.1016/j.envint.2014.06.019.
727
728 Gromet, L.P., Dymek, R.F., Haskin, L.A., Korotev, R.L., 1984. The “North American shale
729 composite”: its compilation, major and trace element characteristics. Geochim.
730 Cosmochim. Acta 48, 2469–2482.
731
732 Ku, T.L., Knauss, K.G., Mathieu, G.G., 1977. Uranium in open oceans, concentration and
733 isotopic composition. Deep-Sea Research 24, 1005-1017.
734
735 Lanceleur, L., Schäfer, J., Blanc, G., Coynel, A., Bossy, C., Baudrimont, M., Glé, C., Larrose,
736 A., Renault, S., Strady, E., 2012. Silver behaviour along the salinity gradient of the
737 Gironde Estuary. Environ. Sci. Poll. Res. 20, 1352-1366. https://doi.org/10.1007/s11356-
738 012-1045-3.
739
740 Langmuir, D., 1978. Uranium solution-mineral equilibria at low temperatures with
741 applications to sedimentary ore deposits. Geochim Cosmochim Acta 42, 6, 547-569.
742
743 Law, S., Turner, A., 2011. Thallium in the hydrosphere of south west England. Environ.
744 Poll. 159, 3484–3489. https://doi.org/10.1016/j.envpol.2011.08.029.
745

746 Lawrence, M.G., Kamber, B.S., 2006. The behavior of the rare earth elements during
747 estuarine mixing-revisited. Mar. Chem. 100, 147–161.
748 https://doi.org/10.1016/j.marchem.2005.11.007.
749
750 Lis, J., Pasieczna, A., Karbowska, B., Zembrzuski, W., Lukaszewski, Z., 2003. Thallium in
751 soils and stream sediments of a Zn-Pb mining and smelting area. Environ. Sci. Technol.
752 37, 4569-4572. https://doi.org/10.1021/es0346936.
753 Liu, R., Lead, J.R., Zhang H., 2013. Combining cross flow ultrafiltration and diffusion
754 gradients in thin-films approaches to determine trace metal speciation in freshwaters.
755 Geochim. Cosmochim. Acta 109, 14–26. http://dx.doi.org/10.1016/j.gca.2013.01.030.
756
757 Luoma, S.N., Ho, Y.B., Bryan, G.W., 1995. Fate, bioavailability and toxicity of silver in
758 estuarine environments. Mar. Pollut. Bull. 31, 44-54. https://doi.org/10.1016/0025-
759 326X(95)00081-W.
760
761 Ma, L., Dang, D.H., Wang, W., Evans, R.D., Wang, W.X., 2019. Rare earth elements in the
762 Pearl River Delta of China: potential impacts of the REE industry on water, suspended
763 particles and oysters. Environ. Pollut. 244, 190–201.
764 https://doi.org/10.1016/j.envpol.2018.10.015.
765
766 Machado, A.A.S, Spencer, K., Kloas, W., Toffolon, M., Zarfl, C., 2016. Metal fate and
767 effects in estuaries: a review and conceptual model for better understanding of toxicity.
768 Sci. Total Environ. 541, 268-281. https://doi.org/10.1016/j.scitotenv.2015.09.045.
769
770 Mangal, V., Zhu, Y., Shi, Y.X., Gueguen, C., 2016. Assessing cadmium and vanadium
771 accumulation using diffusive gradient in thin-films(DGT) and phytoplankton in the
772 Churchill River estuary, Manitoba. Chemosphere 163, 90-98.
773 https://doi.org/10.1016/j.chemosphere.2016.08.008.
774
775 Menegario, A.A., Yabuki, L.N.M., Luko, K.S., Williams, P.N., Blackburn, D.M., 2017. Use
776 of diffusive gradient in thin films for in situ measurements: a review on the progress in
777 chemical fractionation, speciation and bioavailability of metals in waters. Anal.

778 Chim. Acta 983, 54–66. https://doi.org/10.1016/j.aca.2017.06.041.
779
780 Mihajlovic, J., Giani, L., Stärk, H.J., Rinklebe, J., 2014. Concentrations and geochemical
781 fractions of rare earth elements in two different marsh soil profiles at the North Sea,
782 Germany. J. Soil Sediment 14, 1417-1433. https://doi.org/10.1007/s11368-014-0895-3.
783
784 Mihajlovic, J., Stärk, H.J., Rinklebe, J., 2017. Rare earth elements and their release
785 dynamics under pre-definite redox conditions in a floodplain soil. Chemosphere 181,
786 313–319. https://doi.org/10.1016/j.chemosphere.2017.04.036.
787
788 Montero, N., Belzunce-Segarra, M.J., Gonzalez, J.L., Larreta, J., Franco, J., 2012.
789 Evaluation of diffusive gradients in thin-films (DGTs) as a monitoring tool for the
790 assessment of the chemical status of transitional waters within the Water Framework
791 Directive. Mar. Pollut. Bull. 64 (1), 31-39.
792 https://doi.org/10.1016/j.marpolbul.2011.10.028.
793
794 Moreno-Garrido, I., Pérez, S., Blasco, J., 2015. Toxicity of silver and gold nanoparticles
795 on marine microalgae. Mar. Environ. Res. 111, 60-73.
796 https://doi.org/10.1016/j.marenvres.2015.05.008.
797
798 Nielsen, S.P., 2004. The biological role of strontium. Bone 35, 583-588.
799 https://doi.org/10.1016/j.bone.2004.04.026.
800
801 Nieto, J.M, Sarmiento, A.M, Olías, M., Cánovas, C.R, Riba, I., Kalman, J., Delvalls T.A,
802 2007. Acid mine drainage pollution in the Tinto and Odiel Rivers (Iberian Pyrite Belt, SW
803 Spain) and bioavailability of the transported metals to the Huelva estuary. Environ. Int.
804 33, 445–455. https://doi.org/10.1016/j.envint.2006.11.010.
805
806 NIST, 2004. In: Martell, A.E., Smith, R.M. (Eds.), NIST Standard Reference Database 46
807 Version 8.0, Gaithersburg, USA.
808

809 Nozaki, Y., Lerche, D., Alibo, D.S., Tsutsumi, M., 2000. Dissolved indium and rare earth
810 elements in three Japanese rivers and Tokyo Bay: evidence for anthropogenic Gd and in.
811 Geochem. Cosmochim. Acta 64, 3975-3982. https://doi.org/10.1016/S0016-
812 7037(00)00472-5.
813
814 Nozaki, Y., Alibo, D.S., 2003. Importance of vertical geochemical processes in controlling
815 the oceanic profiles of dissolved rare earth elements in the north eastern Indian Ocean.
816 Earth and Planetary Science Letters 205, 155– 172. https://doi.org/10.1016/S0012-
817 821X(02)01027-0.
818
819 Olías, M., Cánovas, C.R., Basallote, M.D., Macías, F., Pérez-López, R., Moreno González,
820 R., Millán-Becerro, R., Nieto, J.M., 2019. Causes and impacts of a mine water spill from
821 an acidic pit lake (Iberian Pyrite Belt). Environ. Pollut. 250, 127-136.
822 https://doi.org/10.1016/j.envpol.2019.04.011.
823
824 Oral, R., Bustamante, P., Warnau, M., D'Ambra, A., Guida, M., & Pagano, G. (2010).
825 Cytogenetic and developmental toxicity of cerium and lanthanum to sea urchin
826 embryos. Chemosphere, 81(2), 194-198.
827 https://doi.org/10.1016/j.chemosphere.2010.06.057
828
829 Panther, J.G., Bennett, W.W., Welsh, D.T., Teasdale, P.R., 2014. Simultaneous
830 measurement of trace metal and oxyanion concentrations in water using diffusive
831 gradients in thin films with a chelex-metsorb mixed binding layer. Anal. Chem. 86, 427-
832 434. https://doi.org/10.1021/ac402247j.
833
834 Parkhurst, D.L., Appelo, C.A.J., 2013. Description of input and examples for PHREEQC
835 version 3.4—a computer program for speciation, batch-reaction, one-dimensional
836 transport, and inverse geochemical calculations. In: U.S. Geological Survey Techniques
837 and Methods, book 6, chap. A43, pp. 497.
838
839 Pérez-López, R., Macías, F., Cánovas, C.R., Sarmiento, A.M., Pérez-Moreno, S.M., 2016.
840 Pollutant flows from a phosphogypsum disposal area to an estuarine environment: an

841 insight from geochemical signatures. Sci. Total Environ. 553, 42–51.
842 https://doi.org/10.1016/j.scitotenv.2016.02.070.
843
844 Ribeiro, C., Couto, C., Ribeiro, A., Maia, A., Santos, M., Tiritan, M., Pinto, E., Almeida, A.,
845 2018. Distribution and environmental assessment of trace elements contamination
846 of water, sediments and flora from Douro River estuary, Portugal. Sci. Total Environ.
847 639, 1381–1393. https://doi.org/10.1016/j.scitotenv.2018.05.234.
848
849 Romero-Freire, A., Joonas, E., Muna, M., Cossu-Leguille, C., Vignati, D.A.L, Giamberini,
850 L., 2019. Assessment of the toxic effects of mixtures of three lanthanides (Ce, Gd, Lu) to
851 aquatic biota. Sci. Total Environ 661, 276–284.
852 https://doi.org/10.1016/j.scitotenv.2019.01.155.
853
854 Rousseau, T.C.C., Sonke, J.E., Chmeleff, J., van Beek, P., Souhaut, M., Boaventura, G.,
855 Seyler, P., Jeandel, C., 2015. Rapid neodymium release to marine waters from lithogenic
856 sediments in the Amazon estuary. Nat. Commun. 6, 7592.
857 https://doi.org/10.1038/ncomms8592.
858
859 Sainz, A., Grande, J.A, de la Torre, M.L. (2004). Characterisation of heavy metal discharge
860 into the Ría of Huelva. Environ. Int. 30, 557-566.
861 https://doi.org/10.1016/j.envint.2003.10.013.
862
863 Sholkovitz, E.R., 1995. The aquatic chemistry of rare earth elements in rivers and
864 estuaries. Aquatic Geochem. 1, 1– 34. https://doi.org/10.1007/BF01025229.
865
866 Tappin, A.D, Barriada, J.L, Braungardt, C.B, Evans, E.H, Patey, M.D, Achterberg, E.P, 2010.
867 Dissolved silver in European estuarine and coastal waters. Water Res 44, 4204–4216.
868 https://doi.org/10.1016/j.watres.2010.05.022.
869
870 Taylor, S.R., McLennan, S.M., 1985. The Continental Crust: Its Composition and
871 Evolution. Blackwell Scientific Publications, Oxford, U.K.
872

873 Turner, A., Turner, D., Braungardt, C., 2013. Biomonitoring of thallium availability in two
874 estuaries of Southwest England. Mar. Pollut. Bull. 69, 172–177.
875 https://doi.org/10.1016/j.marpolbul.2013.01.030.
876
877 Van Geen, A., Boyle, E.A., Moore, W., 1991. Trace metal enrichments in waters of the
878 Gulf of Cadiz, Spain. Geochim. Cosmochim. Acta 55, 2173-2191.
879
880 Verweij, W., 2017. Manual for CHEAQS Next, a Program for Calculating Chemical
881 Equilibria in Aquatic Systems.
882
883 Wang, Z., Yin, L., Xiang, H., Qin, X., Wang, S., 2019. Accumulation patterns and
884 speciesspecific characteristics of yttrium and rare earth elements (YREEs) in biological
885 matrices from Maluan Bay, China: implications for biomonitoring. Environ. Res. 179,
886 108804. https://doi.org/10.1016/j.envres.2019.108804.
887
888 Wen, L.S., Santschi, P.H., Gill, G.A., Paternostro, C.L., Lehman, R.D., 1997. Colloidal and
889 particulate silver in river and estuarine waters of Texas. Environ Sci Tech 31, 723-731.
890 https://doi.org/10.1021/es9603057.
891
892 Windom, H., Smith, R., Niencheski, F., Alexander, C., 2000. Uranium in rivers and
893 estuaries of globally diverse smaller watersheds. Mar. Chem. 68, 307-321.
894 https://doi.org/10.1016/S0304-4203(99)00086-9.
895
896 Wood, C.M., McDonald, M.D., Walker, P., Grosell, M., Barimo, J.F., Playle, R.C., Walsh,
897 P.J., 2004. Bioavailability of silver and its relationship to ionoregulation and silver
898 speciation across a range of salinities in the gulf toadfish (Opsanus beta). Aquat. Toxicol.
899 70, 137–157. https://doi.org/10.1016/j.aquatox.2004.08.002
900
901 Worrall, F., Pearson, D.G., 2001. Water-rock interaction in an acidic mine discharge as
902 indicated by rare earth element patterns. Geochim. Cosmochim. Acta 65,3027 3040.
903 https://doi.org/10.1016/S0016-7037(01)00662-7.
904

905 Yuan, Y., Ding, S., Wang, Y., Zhang, L., Ren, M., Zhang, C., 2018. Simultaneous
906 measurements of fifteen rare earth elements using diffusive gradients in thin films. Anal.
907 Chim. Acta 1031, 98–107. https://doi.org/10.1016/j.aca.2018.05.067.
908
909 **Table Captions**
910
911 **Figure captions**
912 **Figure 1.** Location map of the study area (A), showing the sampling stations (T1-T4) and
913 main anthropogenic activities (B).
914 **Figure 2.** Evolution of dissolved (orange square) line) and particulate (blue circle)
915 concentrations of metals in the estuary for the 4 sampling sites (T1, T2, T3 and T4) and
916 for the 4 sampling times (L: low tide; H: high tide). Tl particulate concentrations were
917 below detection limit of the equipment.
918 **Figure 3.** Percentage of the dissolved and particulate fraction for each metal studied.
919 **Figure 4.** Relationship between the concentration of particulate REE and Y and Ag, and
920 other metals.
921 **Figure 5.** Average speciation values for REE and Y in collected samples.
922
923 **Supplementary Material**
924 **Table SM1.** Basic statistics of physico-chemical parameters, and concentration of major
925 and trace elements of collected samples.
926 **Table SM2.** Basic statistics of the concentration of rare earth elements (REE), Y, Ag, Tl,
927 Cs and U.
928 **Table SM3.** Speciation (average values) of metals studied in collected samples obtained
929 from PHREEQC code (see text for explanation).
930 **Figure SM1.** Relationship between the DGT concentration of metals studied with other
931 elements (obtained from Cánovas et al. 2020).
932 **Figure SM2.** NASC-normalized patterns of dissolved (A), particulate (B) and DGT (C)
933 concentrations of REE.
934 **Figure SM3.** Relationship between the metal concentration in water and in DGT devices.
935 **Figure SM4.** Comparison of REE total concentration in waters and in DGT devices at the
936 different sampling stations.